Journal of Nuclear Materials 384 (2009) 130–139

Contents lists available at ScienceDirect

Journal of Nuclear Materials

journal homepage: www.elsevier.com/locate/jnucmat

UO_2 corrosion in an iron waste package

E.D.A. Ferriss [a,*], K.B. Helean [b], C.R. Bryan [b], P.V. Brady [b], R.C. Ewing [a]

[a] Department of Geological Sciences, The University of Michigan, 2534 C.C. Little, 1100 N. University Avenue, Ann Arbor, MI 48109-1005, USA
[b] Sandia National Laboratories, P.O. Box 5800, MS 0779, Albuquerque, NM 87185-0779, USA

ARTICLE INFO

Article history:
Received 9 June 2008
Accepted 10 November 2008

ABSTRACT

In order to investigate the interactions between spent nuclear fuel, corroding iron waste packages, and water under conditions likely to be relevant at the proposed repository at Yucca Mountain, six small-scale waste packages were constructed. Each package differed with respect to water input, exposure to the atmosphere and temperature. Two of the packages contained 0.1 g UO_2. Simulated Yucca Mountain process water (YMPW) was injected into five of the packages at a rate of 200 μl per day for up to 2 years, at which point the solids were characterized with X-ray powder diffraction, scanning electron microscopy, wet chemistry and electron microprobe analysis. Fe(II) is abundant in the corrosion products that form, and the dominant crystalline product in all cases according to X-ray diffraction is magnetite or the structurally similar maghemite. Minor phases included akaganeite (β-FeOOH) and possibly also hematite (Fe_2O_3), lepidocrocite (γ-FeOOH) and green rust ($Fe(II)_{1-x}Fe(III)_x(OH)_2Y_{x/n}$). Under these conditions, UO_2 is expected to alter to the uranyl silicate uranophane ($Ca[(UO_2)SiO_3(OH)]_2{\cdot}5H_2O$). Neither oxidation of the UO_2 nor any oxidized (uranyl) solid was observed, suggesting that conditions were sufficiently reducing to kinetically hinder U(IV) oxidation.

1. Introduction

Corrosion of iron metal in an enclosed environment is an important phenomenon in both preserving and understanding archeological sites containing iron artifacts (e.g. [1]) and in nuclear waste disposal scenarios, such as those proposed by the United States and Spain, involving a waste package composed primarily of steel. The focus of this paper is the nature of corrosion products of steel waste packages planned for use at the proposed nuclear waste repository at Yucca Mountain (YMR), the local redox and pH conditions inside these waste packages, and the resulting uranium mineralogy and mobility.

Steel and steel corrosion products may play an important role in limiting radionuclide release [2–4]. Uranyl ions (UO_2^{2+}), typical products of the oxidative dissolution of spent nuclear fuel (SNF), may be sorbed by a variety of Fe-bearing minerals including hematite (Fe_2O_3) [5], lepidocrocite (γ-FeOOH) [6], and goethite (α-FeOOH) [6,7] and perhaps also reduced to a less labile form by magnetite (Fe_3O_4) [3,8–13] and green rust ($Fe(II)_{1-x}Fe(III)_x(OH)_2Y_{x/n}$) [14]. Aqueous Fe(II) and steel corrosion products may also immobilize other radionuclide species such as TcO_4^- [15–17], I^- [18] and NpO_2^+ [19].

Corroding steel inside of these waste packages may also influence the redox potential (Eh or pe) and pH, two variables that will strongly influence the degradation behavior of the spent nuclear fuel and the subsequent mobility of radionuclides. Current conceptual models [20] assume that once the waste package has been breached, the system, defined here as the inside of the package, will be flooded with oxygenated water and highly oxidizing air. This situation is unfavorable because oxidizing conditions typically lead to the formation of potentially mobile ions such as TcO_4^-, NpO_2^+ and UO_2^{2+}. The availability of electrons from corroding steel may be an important factor in establishing and maintaining overall reducing conditions. Although the measured system Eh is typically not useful for quantitative predictions [21–25], an overall decrease in redox potential may, depending on water chemistry, stabilize spent nuclear fuel (SNF), kinetically hinder SNF oxidation, or influence the nature of any SNF alteration products.

2. Experiment

2.1. Miniature steel waste packages

Six small-scale (~1:40 by length) miniature waste packages were constructed using 316 stainless steel (nominal composition: $Fe_{62.0}Cr_{18.0}Ni_{14.0}Mo_{3.0}Mn_{2.0}N_{0.08}Si_{0.75}P_{0.045}S_{0.03}C_{0.02}$ [26]), the same material as the proposed Yucca Mountain waste packages [20], for the body, end-caps and fittings (Fig. 1). This steel corrodes less rapidly under most conditions than the A-516 carbon steel (nominal composition: $Fe_{97.87}C_{0.31}Mn_{1.3}P_{0.035}S_{0.035}Si_{0.45}$ [27]) proposed for use as guides for spent nuclear fuel inside the waste packages. The A-516 steel and 316 stainless steels were obtained from Laboratory Testing, Inc., a DOE-approved supplier, and are certified to

* Corresponding author. Tel.: +1 734 615 0656; fax: +1 734 763 4690.
E-mail address: beliza@umich.edu (E.D.A. Ferriss).

0022-3115/$ - see front matter © 2008 Elsevier B.V. All rights reserved.
doi:10.1016/j.jnucmat.2008.11.007

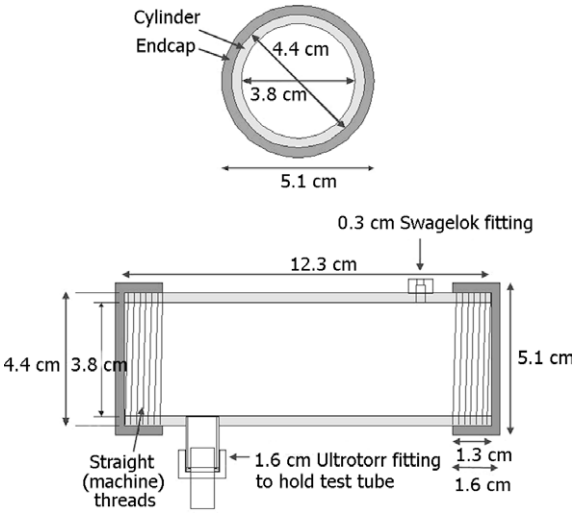

Fig. 1. Schematic of miniature waste package viewed from two angles.

meet the ASTM standards for those materials. Electron microprobe analysis showed that the A-516 steel also contained 0.19 wt% Cr and 0.29 wt% Cu.

In order to maintain the same ratio of body-interior surface area to guide surface area, 25 $1 \times 10 \times 0.1$ cm strips of A-516 carbon steel (mass 7.9 g each) were inserted into each waste package, and inert polytetrafluoroethylene (PTFE) balls with a diameter of 9.53 mm were used to separate the steel strips and fill some of the excess void space. Each package had an internal diameter of 38.1 mm, an internal length of 123 mm, two upper ports (diameter 0.32 mm) and one lower port (diameter 16.0 mm) with an Ultratorr® fitting and a heavy-gauge glass test tube for effluent sample collection. The caps on both ends of each package were sealed using Viton® O-rings and parafilm to prevent higher corrosion rates on the straight-threaded end-caps.

The six packages differed with respect to water input, exposure to the atmosphere, temperature and the presence of uranium (Table 1). In most cases, the upper port on the opposite side from the lower port was covered by a rubber septum for the introduction of the aqueous phase. The exception was package C, which was not injected with water but was left entirely open to an atmosphere with near 100% relative humidity and partial pressures of oxygen and carbon dioxide of $10^{-0.7}$ bar and $10^{-3.4}$ bar, respectively. The second upper ports of packages A, D and E were sealed using a Swagelok snubber, which limits airflow, but allows sufficient exchange to avoid pressurization, while those of packages B and F were left open to the same atmospheric conditions as that of package C. No effort was made to seal the edges around the rubber septum in the upper port. Because of their increased exposure to the atmosphere, the open packages B, C and F were more likely to simulate conditions for a breached waste package at Yucca Mountain. Humid conditions were maintained by enclosing the package setup in a sealed plastic bag and pumping air, which had been saturated with water vapor by bubbling through deionized water, through the bag. A Traceable® digital hygrometer was used to check these conditions. Package D was maintained at 60 °C using a hot plate, and all other packages were allowed to corrode at room temperature. Package D is significantly different from the other three packages because it was initiated as a scoping study, a short test to determine if the steel would corrode quickly under the chosen conditions. Ideally, other packages would be run at elevated temperatures and high relative humidity in order to better gauge the effect of changing these variables.

The uranium in packages E and F was present as synthetic UO_2 prepared from large crystal boules grown from an arc-fusion melt [28] (Fig. 2). The mineral uraninite (naturally occurring UO_2) is considered an excellent analogue for commercial SNF, having the same structure, dominant composition and similar abundant impurities [29]. Although a less appropriate analogue for SNF than uraninite because of a relative lack of impurities, synthetic UO_2 was preferred in this study both in order to simplify the system and to minimize radiation levels associated with decay products such as radon. A small mass (0.1 g) was used in order to further minimize associated radiation, and the UO_2 was crushed using a mortar and pestle, creating sand and silt-sized grains (0.005–2 mm in diameter) to increase available surface area.

2.2. Yucca mountain process water

A simulated Yucca Mountain process water (YMPW) was injected into packages A, B, E and F at a rate of 200 µl per day five days a week using a calibrated needle syringe. Scaling by volume, this rate is equivalent to the introduction of 1.3 ml of water per minute in a full-size waste package. YMPW consists of 50 mg/l silica, 38.3 mg/l Na, enough hydrochloric acid to lower the pH to 7.6,

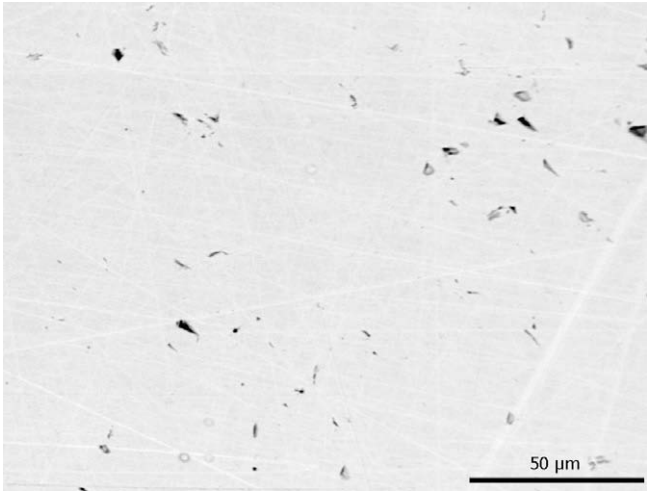

Fig. 2. Secondary electron image of polished cross-section of UO_2 grain prior to crushing for use in miniature waste packages. SEM/EDS of all areas showed only U and O.

Table 1
Test matrix for waste package experiments.

Package	Atmosphere	YMPW volume	Temperature (°C)	Relative humidity	UO_2 present
A	Closed	200 µl/day (~50 ml total)	25	100%	None
B	Open	200 µl/day (~50 ml total)	25	100%	None
C	Open	–	25	100%	None
D	Closed	1 ml/week YMPW-2	60	Environmental	None
E	Closed	200 µl/day–6 months (~25 ml total)	25	100%	0.1 g
F	Open	200 µl/day–7 months (~30 ml total)	25	100%	0.1 g

Table 2
Saturated zone (J-13) [31] and selected pore water compositions [32] compared with initial concentrations in YMPW and YMPW-2.

Component	Unit	J-13	Ca pore water	Na pore water	YMPW[a]	YMPW-2
pH[b]	pH	7.4 (7.8)	7.6 (8.1)	7.4 (8.3)	7.8	7.9
$SiO_{2(aq)}$	mmolar	0.95	0.66	0.66	0.83	0.90
HCO_3^-	mmolar	2.34	6.51	5.93	0.45	1.95
Cl^-	mmolar	0.20	0.59	0.68	1.00	0.02
Na^+	mmolar	1.99	1.70	5.22	1.66	2.00
Ca^{2+}	mmolar	0.32	2.35	2.02	5.02	0.87

[a] All but pH are calculated values given known Na and Si inputs, atmospheric carbon dioxide levels and calcite equilibria. Actual values produced may vary slightly.
[b] Values given in parentheses for J-13 and pore waters assume the solution is equilibrated to log $fCO_2 = -3.0$.

and an excess of powdered calcite. The solution was equilibrated with the atmosphere for five days, filtered, and allowed to equilibrate with the atmosphere for an additional five days. The final pH for different batches stabilized between 7.5 and 7.9. J-13 well water [30,31], pore waters from the unsaturated zone near Yucca Mountain [32] and various calculated waters have been used to approximate the composition of fluids entering a breached waste package. However, there is no universally accepted optimal fluid composition for use in studies of the release of radionuclides at a proposed nuclear waste repository (source term work) because of large uncertainties in, for example, breach time, fluid sources and the extent of prior fluid-rock interactions. The waters currently found at Yucca Mountain are typically highly supersaturated with respect to quartz and approximately saturated with respect to calcite [32], and the major element chemistry of YMPW is similar to these waters (Table 2). Another fluid, YMPW-2, a pH 7.9 dilute Na–Ca-bicarbonate silicate water with approximately 0.8 ppm chloride and 1.0 ppm fluoride, was injected into package D at a rate of 1 ml per week.

2.3. Characterization of solids

Non-radioactive packages were handled primarily at Sandia National Laboratories (SNL), and all work with the U-bearing package (E and F) was performed at the University of Michigan (UM). The surfaces of the A-516 steel and UO_2 were examined using scanning electron microscopy with energy dispersive spectroscopy (SEM/EDS; Hitachi S3200N at UM; JEOL JSM-5900LV at SNL) prior to being placed in the packages. Packages A, B, E and F were allowed to corrode at room temperature and 100% relative humidity until the test tubes in the lower port were nearly full of effluent. Package C was opened at the same time as packages A and B, and package D was sampled at 30 and 90 days. During sampling, the packages were disassembled under inert atmosphere (N_2-filled glove bag at SNL; Coy Laboratories glove box containing a mixture of N_2 and 5% H_2 gas, a desiccant and a catalyst for O_2 combination with H_2 at UM).

Characterization of corrosion products included powder X-ray powder diffraction (XRD, Scintag X1 at UM and Bruker D8-ADVANCE at SNL, Cu Kα radiation), SEM/EDS, electron microprobe analysis (Cameca SX100) with wavelength dispersive spectroscopy (EMPA/WDS), and wet chemical analysis. XRD samples from packages A, B and D were prepared as smear mounts and analyzed within 2 h after the packages were opened. Due to a catastrophic XRD failure at SNL, the original XRD data for package D was lost except for a graphical image, and the samples were analyzed again 3.5 years later at UM. Corrosion products from the U-containing packages E and F were scraped onto a glass slide with a plastic scraper and allowed to dry under inert atmosphere for two hours prior to being analyzed. Strips from packages E and F with relatively high levels of corrosion but low levels of radioactivity were cross-sectioned, given a diamond polish, and examined with SEM/EDS and EMPA/WDS. SEM analyses were conducted at an accelerating voltage of 20 kV, and EMPA/WDS analyses used 25 kV, a beam current of 40 nA and typical counting times of 30 s, except for U Lα, which was run at 50 nA and 300 s to obtain comparable precision to U Mα. The standards used for the calibration were: UO_2 for U Mβ (count time 200 s) and U Lα (count time 300 s), Cu metal for Cu, andradite for Fe and Si and manganotantalite for Mn.

Fe(II)/Fe(III) ratios in the corrosion products were measured using a method combining the standard Pratt and ferrozine wet chemical methods [33,34]. The samples were dissolved in H_2SO_4 and HF rather than HCl [35], and the resulting solution was analyzed using the spectrophotometric agent ferrozine. Two potential weaknesses of all wet chemical methods are: (1) a very small sample may not be representative of the whole, and (2) the Fe(II) can be easily oxidized during sample digestion. In this study, as in the traditional Pratt method, oxidation was prevented by immediate and continuous boiling of the acid mixture during digestion. Given the likelihood of oxidation, the numbers reported for all Fe(II)/Fe(III) ratios are minimum values.

2.4. Water chemistry

Total U and Fe were measured in the effluent of packages E and F using inductively coupled mass spectrometry (ICP-MS, Thermo Fisher Finnigan Mat Element at UM). Effluent pH was analyzed using a Ross electrode with a Symphony SB70P meter, and Fe(II)/Fe(III) values were measured using the ferrozine method [33]. These values, along with initial YMPW water chemistry, were used as input in the software package EQ3NR [36] to calculate speciation, solution-mineral equilibria, pe and oxygen fugacities using a thermodynamic database developed specifically for application to the Yucca Mountain project [37]. The major assumptions that went into these calculations were (1) the concentrations of elements other than Fe (Table 2) remained constant throughout the experiment, (2) K^+ and Al^{3+} are also present due to the groundwater interaction with the surrounding tuff at Yucca Mountain and (3) all aqueous and gas phases have reached thermodynamic equilibrium. Assumption three is rarely correct in natural waters [21–25] and is almost certainly incorrect here. Aqueous Fe(II)/Fe(III) ratios may have been controlled primarily by the rates of Fe corrosion, precipitation and sorption. The calculated oxygen fugacities and pe's determined and reported here based on the Fe(II)/Fe(III) redox couple should be considered only estimates of a theoretical system pe that may bear little resemblance to the actual potential of the U(IV)/U(VI) couple.

3. Results

3.1. Fe speciation and pe–pH conditions

Fig. 3 shows the pe–pH conditions inside of the packages determined from the measured pH and Fe(II)/Fe(III) ratio in the effluent

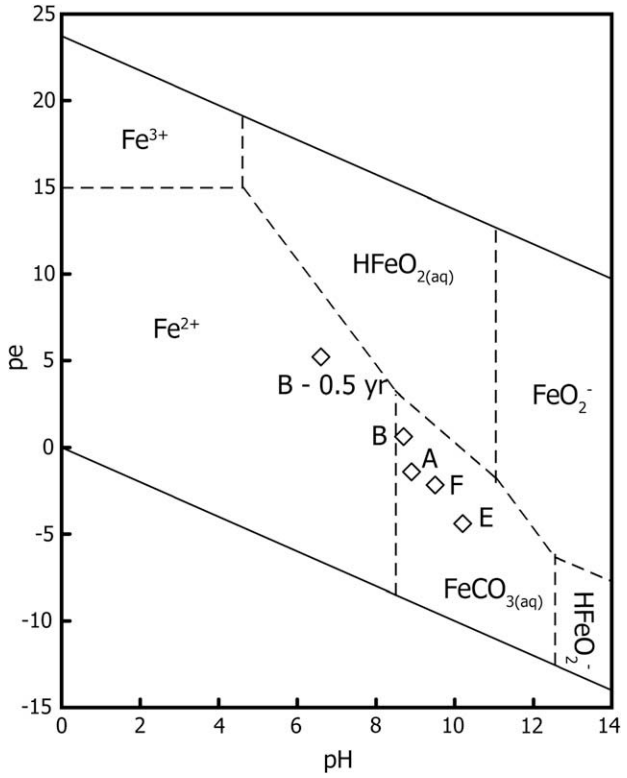

Fig. 3. pe–pH diagrams showing package chemistry (letters explained in Table 3) and dominant aqueous Fe phases in the effluents.

(Table 3) and superimposed on the pe–pH diagrams for aqueous Fe species in the effluent. Over time, the internal chemistry becomes both more basic and more reducing as the steel corrodes, releasing more electrons from the iron. The open packages are more oxidizing than similar closed packages. Aqueous species were chosen for the pe–pH diagram based on the results of EQ3NR speciation calculations (Table 4). Calculated aqueous Fe species include $HFeO_{2(aq)}$, FeO_2^-, Fe^{2+}, $HFeO_2^-$ and $FeOH^+$, and in most packages, $FeCO_{3(aq)}$ is the dominant aqueous Fe species after 1.5 years. Siderite ($FeCO_{3(s)}$) has extremely sluggish precipitation kinetics [38] and was not observed.

3.2. Metal corrosion products

The extent of metal corrosion varied from virtually nothing, most notably in package C, which was not injected with water, to up to 50% on some strips. Typically 5% or less of an individual strip appeared corroded. EDS analysis showed a major chemistry of Fe or Fe–O in all areas, but Cu, S, Si and Mn were also noted in

Table 4
Activity (mM) of aqueous Fe species in packages calculated by EQ3NR.

Species	A (closed)	B 0.5 year	B 1.5 year	E (U-closed)	F
$HFeO_{2(aq)}$	5.04E-07	7.85E-06	1.05E-05	2.77E-06	7.67E-06
FeO_2^-	1.17E-07	Negligible	1.54E-06	1.29E-05	6.59E-06
FeO^+	Negligible	5.48E-06	Negligible	Negligible	Negligible
$FeCO_{3(aq)}$	1.45E-06	1.79E-07	8.04E-07	8.53E-06	8.61E-06
Fe^{2+}	3.61E-07	1.22E-05	3.09E-07	2.77E-07	6.76E-07
$HFeO_2^-$	Negligible	Negligible	Negligible	4.77E-06	Negligible
$FeOH^+$	1.01E-07	Negligible	5.43E-08	1.51E-06	7.02E-07

corrosion products. EMPA/WDS results of the corrosion products also show a high level of heterogeneity (Fig. 4). This variability in chemistry suggests that solid samples taken for XRD (a few tens of mg) and wet chemical analyses (about 5 mg) may not be representative. To minimize this problem, multiple analyses were performed when a sufficient mass of corrosion products was available.

The major corrosion product identified by XRD in packages A, B, D, E, and F was either magnetite, Fe_3O_4, or the structurally similar maghemite, Fe_2O_3 (Fig. 5). Wet chemical analyses of corrosion products from all of the packages (Table 3) confirmed the presence of Fe(II), which suggests the dominant corrosion product is magnetite rather than maghemite. However, given that the Fe(II)/Fe(III) ratio in the bulk solids is greater than that of magnetite (0.5) at least one other reduced Fe phase must be present. Because no other significant peaks appeared in the XRD spectra, this phase is probably amorphous. It is also possible that maghemite is the dominant corrosion product, and all of the Fe(II) was present in poorly crystalline phases.

There is XRD evidence for akaganeite in packages A, B and F. Akaganeite is nominally β-FeOOH but is perhaps better described as $\beta\text{-}FeO_{1-2x}(OH)_{1+x}Cl_x$ because Cl^- or F^- ions are typically present [39]. Formation of akaganeite is associated with corrosion processes induced by Cl^- ions [40]. Small lepidocrocite (γ-FeOOH) peaks were observed in packages E and F after 2 years, and one peak suggesting the presence of hematite (Fe_2O_3) was observed in package D after 90 days. An unidentified phase with a large *d*-spacing of 13 Ångstroms was noted in the initial survey of package D, the high temperature study. This mineral may correlate with a platy Fe–O–Cl phase that was noted using SEM/EDS (Fig. 6). The layered structure, high Fe(II) to Fe(III) ratio, Cl-content, and evidence of lepidocrocite formation in packages E and F suggest the presence of the layered Fe-oxyhydrate green rust [41], which has also been noted as a corrosion product of zero-valent iron reactive barriers [42].

The results of this study are in general agreement with previous studies of Fe and steel corrosion, in which magnetite is typically the dominant phase. Maghemite, goethite, lepidocrocite, hematite, siderite and green rust may also be present, depending on experimental conditions, such as relative humidity, water chemistry,

Table 3
Measured solid corrosion product Fe(II)/Fe(III) ratios, effluent Fe(II) and Fe(III) values[a] and pH, as well as pe and log oxygen fugacity (fO_2) calculated using the geochemical modeling tool EQ3NR.

Package	Sample time	Solids[b] Fe(II)/Fe(III)	$[Fe(II)_{(aq)}]$ (μg/l)	$[Fe(III)_{(aq)}]$ (μg/l)	pH	pe	Log fO_2
A (closed)	1.5 years	0.72	11	3.1	8.9	−1.4	−53.0
B (open)	1.5 years	0.60 (±0.05)	6.4 (±3.6)	60. (±6)	8.7	0.63	−45.6
B	0.5 years	ND[c]	38 (±2)	58 (±2)	6.6	5.21	−35.7
D (heated)	90 days	0.04	ND	ND	ND	ND	ND
E (Uclosed)	2 years	0.90 (±0.3)	88	77	10.2	−4.39	−59.7
F (Uopen)	2 years	1.5 (±0.4)	62	70	9.5	−2.16	−53.7

[a] When enough material for multiple samples was available, error estimates were made.
[b] These are minimum values in all cases. Because of a delay in transferring the sample during preparations for titration, package D is particularly likely to have experienced oxidation.
[c] ND stands for 'not determined'.

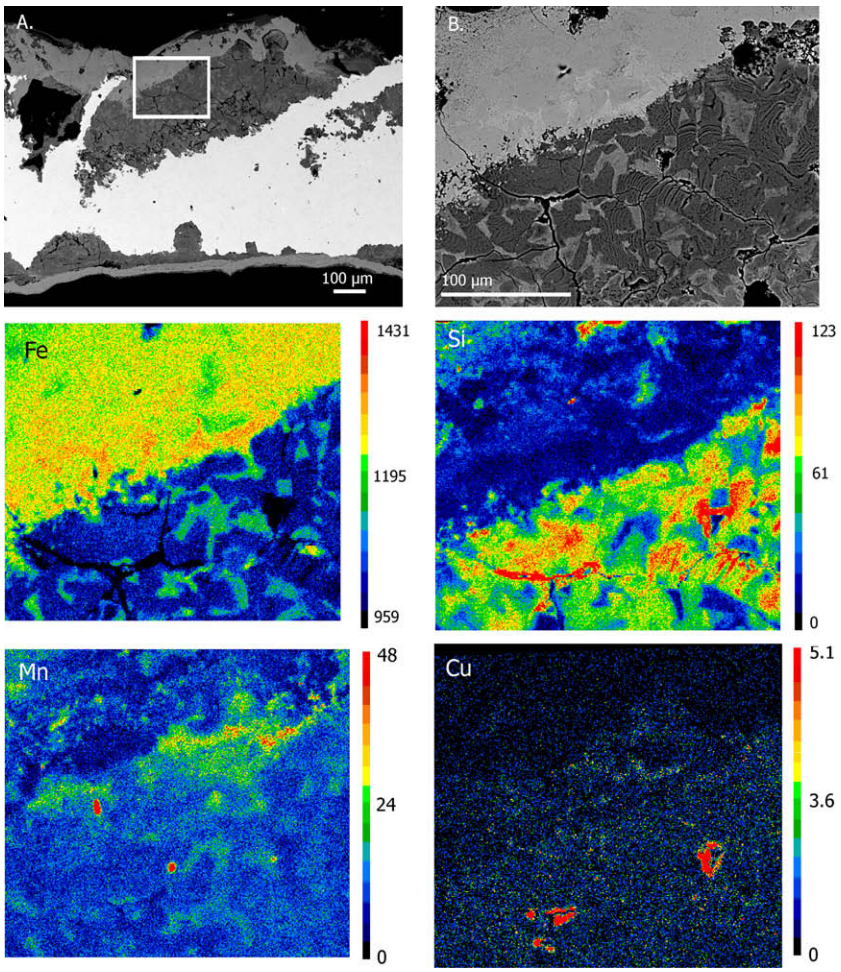

Fig. 4. BSE images of corroded steel from package E showing iron corrosion products. Bright areas in A are largely uncorroded steel, and the darker phases consist of Fe oxides, most likely magnetite. The boxed area of A is shown magnified in B. Electron microprobe analysis with WDS was used to create elemental maps of the boxed area in A. These are shown labeled by element. Map scale bars show total counts per pixel.

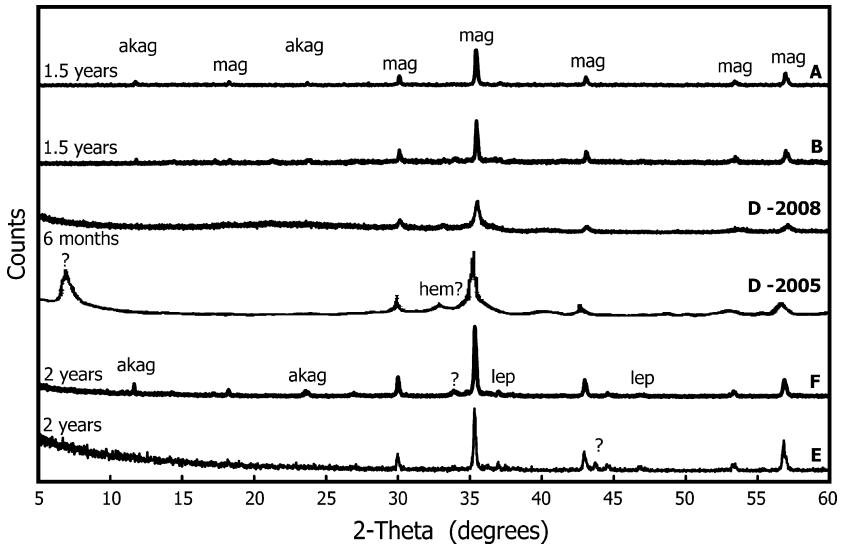

Fig. 5. X-ray diffraction spectra (Cu Kα radiation) of corrosion products in packages A, B, D, F, and E showing magnetite/maghemite (mag), hematite (hem), akaganeite (akag), lepidocrocite (lep), and an unidentified mineral (?). All patterns were obtained within 6 h of opening the packages except D-2008, which was obtained 3.5 years after the initial analysis. The original data for the high temperature study (D-2005) has been lost, and all peak positions for that pattern should be treated as approximate values.

steel composition, time and temperature [12,43–56]. Bench-top experiments, even those such as the current study that were run over a series of years, are short-term compared to the life of a repository. Corrosion studies of archeological artifacts suggest that

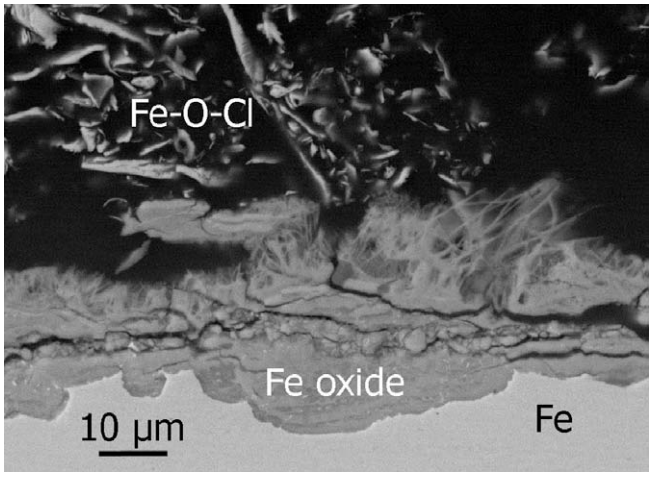

Fig. 6. Backscattered electron micrographs of Package D corroded steel of at 90 days. The polished cross-section shows oxidized areas along the steel surface and loosely consolidated fibers or plates of a Cl-rich phase.

magnetite, goethite and maghemite are the most important long-term corrosion products, although akaganeite, lepidocrocite and siderite have also been found as corrosion products of iron artifacts in certain environments. Unfortunately, these studies are not sufficiently well developed to be useful for quantitative long-term corrosion modeling [57,58].

Under anoxic conditions, the reduction of H^+ becomes important [59], and the corrosion of Fe is typically thought of as a transformation first to $Fe(OH)_2$ followed by oxidation to magnetite via the Schikorr reaction [60]:

$$3Fe(OH)_2 \rightarrow Fe_3O_4 + H_2 + 2H_2O \quad (1)$$

Given the very low redox potentials, it is possible that there may also have been some accumulation of hydrogen, but the lack of XRD evidence for $Fe(OH)_2$ formation suggests that the Schikorr reaction was of minor importance.

Copper, which was observed to be a minor constituent of the original A-516 steel strips used in this study, migrated out of the steel during corrosion and formed distinctive small balls highly enriched in Cu (Fig. 7). While the Cu balls are very common in the cracks and crevices throughout the corroded steel, they do not appear to be interacting with the U directly. The potential effects of Cu and other minor components in the steel on the corrosion of UO_2 under these conditions were not evaluated.

3.3. Corrosion of UO_2

Several particles containing U and O were found with SEM/EDS associated with the corrosion products. Most of these were only a few μm wide (Fig. 8), although one 20 μm-wide grain was located. Because of the small size of the grain, microscale characterization, for instance with transmission electron microscopy, could not be carried out, but elemental maps and line scans were generated around the grain using EMPA/WDS (Fig. 9). Measured wt% UO_2 for points on the grain were close to 100, and lower wt% for certain points on the UO_2 corresponded to low total measured wt% (holes). These pores on the surface of the grain are similar to those observed in original grains (Fig. 2) and may have increased in size during the polishing process. The broken areas of the grain along an otherwise sharp boundary may also be a result of polishing.

Weight percentages of 0.3–0.1% UO_2 were observed with EMPA/WDS up to 15 μm from the grain. These results may have been caused by (1) secondary fluorescence of the U in the grain by Fe, (2) the remainder of the grain being buried just below the surface,

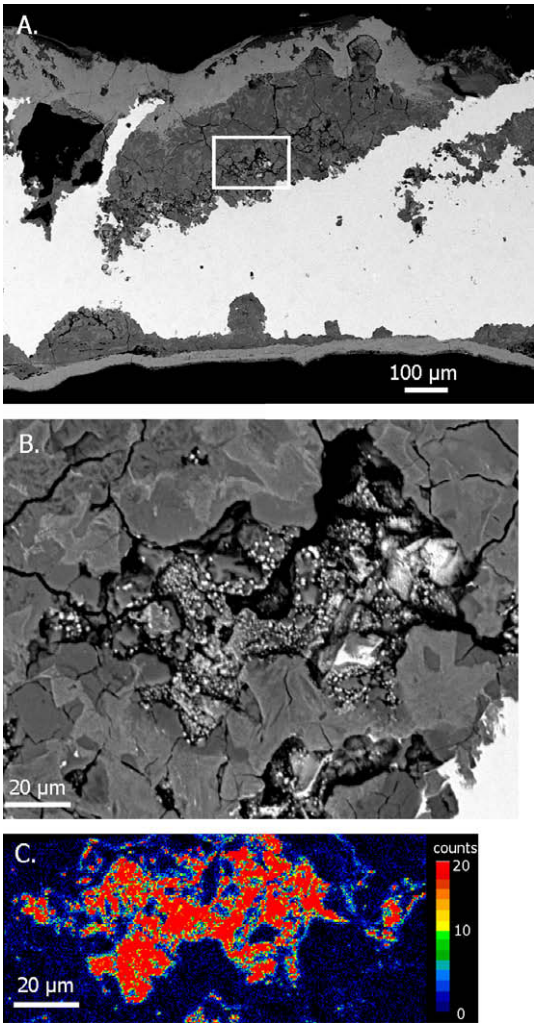

Fig. 7. Backscattered electron images of a steel strip cross-sections from package E. The bright phases in the boxed area of A are shown magnified in B. Electron microprobe analysis was used to generate an elemental map of Cu, shown in C. Elemental map scale bar shows total counts per pixel.

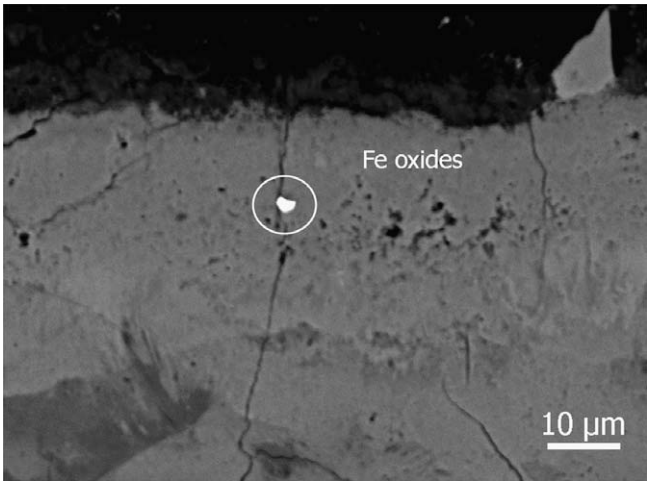

Fig. 8. Back-scattered electron image of a typical small UO_2 fragment (circled and identified by EDS) found in the package E after 2 years. No other solid uranium phases were detected using SEM/EDS, XRD, or EMPA.

(3) poor resolution of spot size during EMPA measurements, or (4) migration of U from the grain and association with iron corrosion

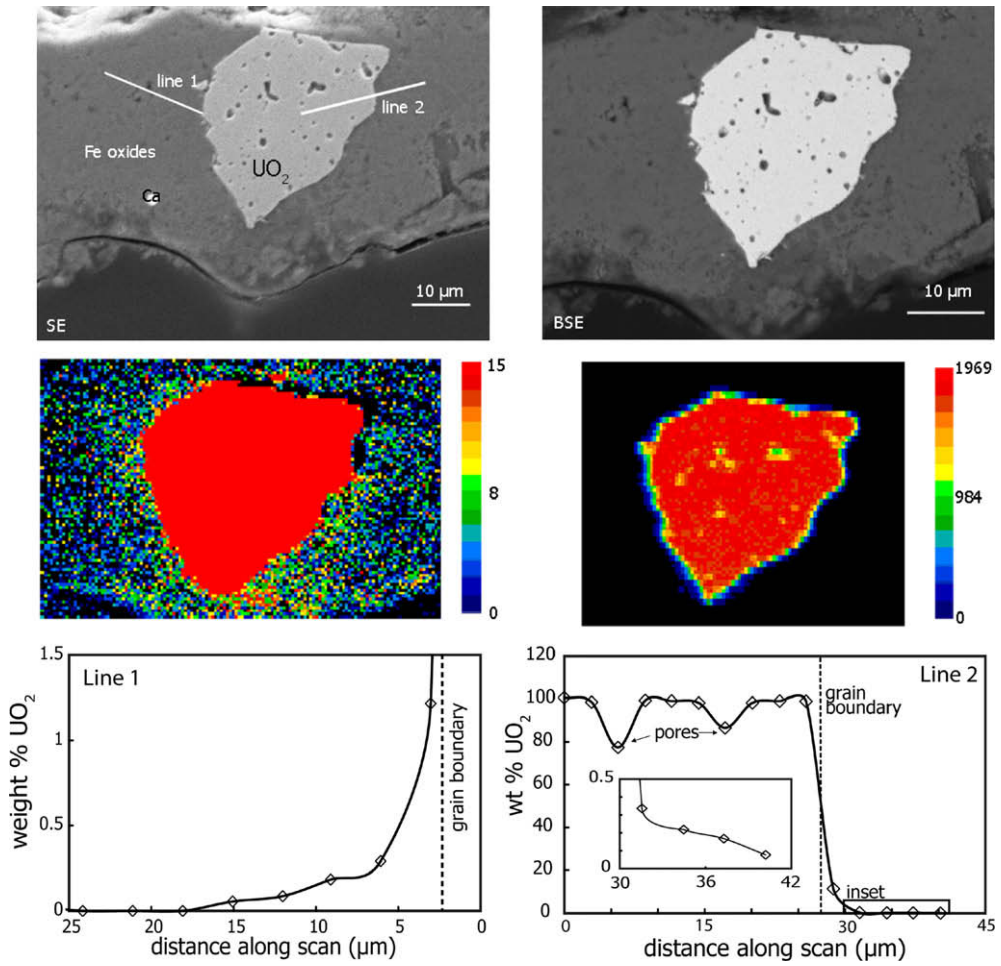

Fig. 9. Secondary electron (SE) and back-scattered electron (BSE) image of UO_2 grain surrounded by steel corrosion products (most likely magnetite) in package E with associated EMPA/WDS line scans and elemental maps of U focused at different levels of total counts per pixel.

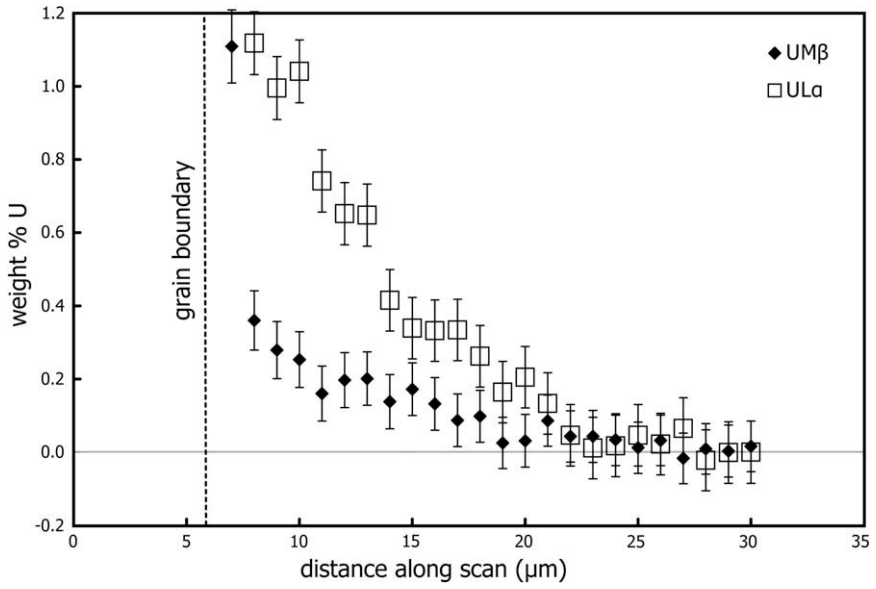

Fig. 10. EMPA/WDS line scans of U Lα and Mβ taken near line 1 of the UO_2 grain shown in Fig. 9. Vertical error bars represent one standard deviation in the measured wt% U.

products. If the U Mβ lines were being fluoresced by Fe, weight percent U measured using Mβ lines should be higher than weight percent U measured using Lα lines. A comparison of quantitative results for U Lα (25 kV, 50 nA, 300 s count time) and Mβ lines (20 kV, 20 nA, 20 s count time) indicates that this is not the case (Fig. 10), and therefore secondary fluorescence is not an important

phenomenon in this system. The similarities in line scans on two different sides of the grain and fairly sharp grain boundary suggest that either the buried grain is highly symmetrical or counts from buried UO_2 are negligible. Because the grain may not be well anchored in the corrosion products, the sample was not polished an additional 1 μm for a definitive test. Resolution of the spot size could not be determined without modeling software or comparison to a similar sample known to have a very sharp grain boundary. If EMPA/WDS measurements do correctly indicate the presence of U surrounding the original grain, the U may be present as (1) a reprecipitated uranium mineral such as UO_2, as was observed in a recent study with iron nanoparticles [61], (2) uranyl ions absorbing to magnetite or other iron oxide surfaces, or (3) part of a poorly crystalline phase.

Although the exact nature of the U–Fe association cannot be made clear without more detailed nanoscale analysis such as with transmission electron microscopy (which cannot be applied due to the small size of the sample), the low values of U associated with the iron corrosion products, generally sharp appearance of the boundary between the grain and surrounding corrosion products, and low concentration of dissolved U in the water (0.868 ppb in package E and 4.536 ppb in package F) strongly suggest that overall UO_2 corrosion was minimal.

4. Discussion

4.1. Lowered redox conditions

The heterogeneity of the corrosion products and presence of uncorroded steel demonstrates that even after 2 years, the solids are far from thermodynamic equilibrium. The pe–pH conditions for all packages plot in the hematite, not magnetite, stability field (Fig. 11). Therefore, calculated pe conditions, which are based on only the aqueous Fe(II)/Fe(III) ratio without regard to the possible influence of solid iron phases, should be taken as estimates.

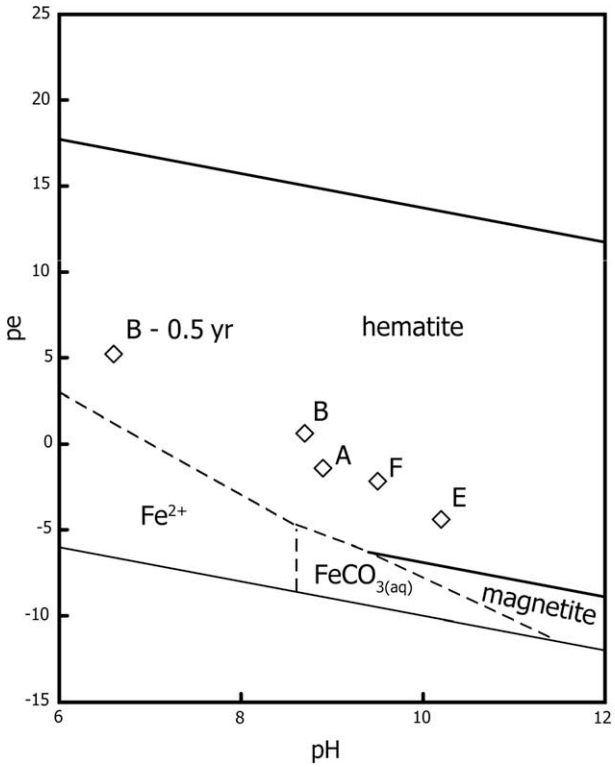

Fig. 11. Close-up of measured redox and pH conditions inside of the packages (letters explained in Table 3) superimposed on the field of iron minerals expected to be most thermodynamically stable in YMPW. The activity of Fe is taken as 1.7×10^{-6} M, an average measured value.

The high Fe(II)/Fe(III) ratios in the package effluent (assuming Fe redox chemistry dominates the system) and negligible UO_2 corrosion suggest that the internal chemistry of the packages is much more reducing than the outside air. This is likely due to a combination of low oxygen transport rates into the packages relative to Fe and U oxidation reactions (which remove oxygen from the system through the formation of magnetite and other oxides or oxyhydroxides) and the presence of a buffering system that resists the Eh change that would be expected when oxygen enters the system.

Although the packages were filled with air initially and allowed some contact with the surrounding environment, the rate of oxygen transport into the packages was a controlling factor. The higher value of dissolved U in package F as compared with package E indicates a greater degree of oxidative dissolution of the UO_2, which follows directly from the greater access to oxygen through the open port (assuming no uranyl phases precipitated in either case). An identical experiment conducted with one side left completely open would be expected to show far higher levels of both Fe and U corrosion (this would be an appropriate control in future experiments).

As Fe oxidation proceeds, equilibrium reactions involving secondary phases may also play a role. A buffer is traditionally defined as a system that resists changes in pH (e.g., a mixture of roughly equal proportions of a weak acid and its conjugate base) or Eh (e.g., the magnetite-hematite buffer). Equilibrium lines for these reactions plot on Pourbaix diagrams as vertical and horizontal lines, respectively. If both products and reactants of a given reaction involving both redox and pH changes are present in a system, they may create a buffer that resists deviations in the system away from the equilibrium line. The measured pe–pH points for the packages form a rough line with a slope of approximately 1 e^- to 3 H^+, suggesting a buffering system with rapid kinetics relative to other reactions in this system.

The relative importance of above processes may have changed over the course of the experiment. Perhaps Fe(III) phases such as ferrihydrite (poorly crystalline $Fe(OH)_3$), akaganeite (β-FeOOH), or lepidocrocite (γ-FeOOH) formed early, when oxygen was relatively abundant in the packages and corrosion rates may have been more rapid, and then slowly dissolved or converted to Fe(II)-bearing species after oxygen became depleted. This would explain the general increase in the Fe(II)/Fe(III) ratios of the solid corrosion products over time, and depending on the reaction, may also account for the observed pH increase as in the following equation:

$$3FeOOH + H^+ + e^- \rightarrow Fe_3O_4 + 2H_2O \quad (2)$$

If O_2(aq) is sufficiently depleted, Fe(III) species may be the most important oxidizing agents in the system.

4.2. Kinetic hindrance of UO_2 corrosion

The predicted speciation of U depends on the water chemistry. In YMPW, which contains high levels of both Ca^{2+} and silica (Table 2), geochemical modeling using the Yucca Mountain project thermodynamic database [37] predicts that under all pe–pH conditions tested uranophane ($Ca[(UO_2)SiO_3(OH)]_2{\cdot}5H_2O$) is the thermodynamically stable phase. Uranophane has been noted as a corrosion product of uraninite/UO_2 under oxidizing conditions [62,63].

The above thermodynamic prediction should be taken only as a starting point, both because of likely kinetic effects and because errors in thermodynamic measurements may lead to large changes in the calculated stability field [64]. The thermodynamic data for coffinite, which is known to be an important alteration product

of uraninite under reducing and Si-rich conditions [65], is especially problematic. Although coffinite was first synthesized over 50 years ago [66–68], no calorimetric studies have been performed because of difficulties synthesizing a large enough pure sample [69], and available thermodynamic data for coffinite is generally not considered valid [70]. Also, this database does not include becquerelite ($Ca(UO_2)_6O_4(OH)_6{\cdot}8(H_2O)$), which is expected to be one of the most important phases in the UO_3–CaO–H_2O system [71].

The UO_2 grains in these experiments are not expected to be thermodynamically stable with the oxygenated fluids of the experiments, and their persistence indicates that oxidation was kinetically hindered. The decrease in measured redox conditions reflects a decrease in availability of the chemical reactant O_2, and limited reactant availability leads to slower reaction times. A layer of corrosion products surrounding the UO_2 grains may also have contributed by forming a protective barrier against oxygen and water.

4.3. Implications for radionuclide release from waste packages

Standard conceptual models used in performance assessment analyses consider only two possible scenarios in the lifetime of the waste package: before breach, when no water is available and the corrosion rate is negligible, and after breach, when water infiltrates the package and the spent nuclear fuel (SNF) is exposed to the open air and oxidized relatively quickly [20]. The results of this study suggest that a more accurate description of the rate of oxidative corrosion of spent nuclear fuel at the proposed repository site at Yucca Mountain should include at least one intermediate stage: when the steel begins to corrode, conditions inside of the canister are more reducing, and SNF does not corrode significantly.

Given the many tons of carbon and stainless steel within the actual waste packages, reducing conditions are certain to exist inside of the waste package for some time, but any estimate of that time that is based only on these short-term experiments is unlikely to be meaningful. The relative rates of oxygen ingress and steel oxidation will be largely determined by the form and extent of the breach and the rate of water flow into the package, both of which may change over time. Even assuming a constant water flow and breach size, these experiments are too short in duration to determine any relation between the complete oxidation of carbon steel (expected in tens to hundreds of thousands of years [72]) and final redox chemistry. Oxidizing conditions may, for instance, become established well before all of the carbon steel has corroded if the breached area is large, or reducing conditions may persist long afterwards due to the effect of corrosion of the stainless steel container or the formation of a protective layer of corrosion products.

The low oxygen fugacities of this study (Fig. 11) were measured for a steel type that corrodes relatively easily. Stainless steel, which has been proposed to replace carbon steel in the waste packages [20], corrodes more slowly. Depending on the rate of fluid flow, use of this steel may either extend the period of lowered redox chemistry or, if the steel is sufficiently corrosion resistant, may not contribute to reducing conditions at all.

The effectiveness of corrosion products such as magnetite and hematite as radionuclide getters will depend on the water chemistry, particularly the carbonate concentration and pH. Uranyl ions are known to form highly mobile carbonate complexes such as $(UO_2)_2CO_3(OH)_3^-$, $UO_2CO_3^\circ$, $UO_2(CO_3)_2^{2-}$ and $UO_2(CO_3)_3^{4-}$ [73], which are not easily adsorbed onto Fe oxides or other mineral surfaces [5,74–78]. High carbonate concentrations, which may also increase the mobility of NpO_2^+ [79], are expected at Yucca Mountain, and basic waters like those found in the packages will facilitate carbonate complex formation. However, over much longer time scales, corrosion modeling suggests that pH will be acidic, minimizing the importance of uranyl carbonate complexation [32].

5. Conclusions

This study examined the corrosion products of A-516 steel and synthetic UO_2 over a 2 year period under conditions likely to prevail at the proposed nuclear waste repository at Yucca Mountain shortly after the waste package is breached. Over this time period, approximately 5% of the steel interacting with water experienced some degree of corrosion, and the redox potential for the Fe(II)/Fe(III) couple decreased steadily. The UO_2 did not experience significant alteration, suggesting that for several years after breach, spent nuclear fuel corrosion and radionuclide release will be minimal.

Acknowledgments

The authors thank an anonymous reviewer for constructive comments that lead to a substantial improvement in the manuscript, as well as Artur Deditius, Carl Henderson, and Eric Essene for help with the EMPA/WDS and SEM/EDS. EDA Ferriss is thankful for fellowships from the Office of Civilian Radioactive Waste Management and the National Science Foundation. This work was supported by the Office of Science and Technology and International (OST&I) of the Office of Civilian Radioactive Waste Management (DE-FE28-04RW12254) and NSF EAR 99-11352. The views, opinions, findings and conclusions or recommendations of the authors expressed herein do not necessarily state or reflect those of DOE/OCRWM/OSTI. Sandia is a multiprogram laboratory operated by Sandia Corporation, a Lockheed Martin Company, for US DOE's NNSA under contract DE-AC04-94AL85000.

References

[1] W. Gerwin, R. Baumhauer, Geoderma 96 (2000) 63.
[2] C.W. Eng, G.P. Halada, A.J. Francis, C.J. Dodge, J.B. Gillow, Surf. Interface Anal. 35 (2003) 525.
[3] C.J. Dodge, A.J. Francis, J.B. Gillow, G.P. Halada, C. Eng, C.R. Clayton, Environ. Sci. Technol. 36 (2002) 3504.
[4] B. Gu, L. Liang, M.J. Dickey, X. Yin, S. Dai, Environ. Sci. Technol. 32 (1998) 3366.
[5] C.H. Ho, N.H. Miller, J. Colloid Interface Sci. 110 (1986) 165.
[6] L.N. Moyes, R.H. Parkman, J.M. Charnock, D.J. Vaughan, F.R. Livens, C.R. Hughes, A. Braithwaite, Environ. Sci. Technol. 34 (2000) 1062.
[7] D.M. Sherman, C.L. Peacock, C.G. Hubbard, Geochim. Cosmochim. Acta 72 (2008) 298.
[8] T.B. Scott, G.C. Allen, P.J. Heard, M.G. Randell, Geochim. Cosmochim. Acta 69 (2005) 5639.
[9] B. Grambow, E. Smailos, H. Geckeis, R. Muller, H. Hentschel, Radiochim. Acta 74 (1996) 149.
[10] T. Missana, U. Maffiotte, M. Garcia-Gutierrez, J. Colloid Interface Sci. 261 (2003) 154.
[11] M. Rovira, S. El Aamrani, L. Duro, J. Gimenez, J. de Pablo, J. Bruno, J. Hazard. Mater. 147 (2007) 726.
[12] D.S. Dunn, M.B. Bogart, C.S. Brossia, G.A. Cragnolino, Corrosion 56 (2000) 470.
[13] L. Duro, S. El Aamrani, M. Rovira, J. de Pablo, J. Bruno, Appl. Geochem. 23 (2008) 1094.
[14] E.J. O'Loughlin, S.D. Kelly, R.E. Cook, R. Csencsits, K.M. Kemner, Environ. Sci. Technol. 37 (2003) 721.
[15] J.M. Zachara, S.M. Heald, B.H. Jeon, R.K. Kukkadapu, C.X. Liu, J.P. McKinley, A.C. Dohnalkova, D.A. Moore, Geochim. Cosmochim. Acta 71 (2007) 2137.
[16] D.Q. Cui, T.E. Eriksen, Environ. Sci. Technol. 30 (1996) 2263.
[17] S.E. Pepper, D.J. Bunker, N.D. Bryan, F.R. Livens, J.M. Charnock, R.A.D. Pattrick, D. Collison, J. Colloid Interface Sci. 268 (2003) 408.
[18] M. Fuhrmann, S. Bajt, M.A.A. Schoonen, Appl. Geochem. 13 (1998) 127.
[19] A.Y. Teterin, K.I. Maslakov, Y.A. Teterin, S.N. Kalmykov, K.E. Ivanov, L. Vukcevic, A.B. Khasanova, N.S. Shcherbina, Russ. J. Inorg. Chem. 51 (2006) 1937.
[20] SNL, Total System Performance Assessment Data Input Package for Requirements Analysis for Transportation Aging and Disposal Canister and Related Waste Package Physical Attributes Basis for Performance Assessment, Sandia National Laboratories, 2007, TDR-TDIP-ES-000006 Rev 00.
[21] J.C. Morris, W. Stumm, in: W. Stumm (Ed.), Equilibrium Concepts in Natural Water Systems, Advances in Chemistry Series, vol. 67, American Chemical Society, Washington, DC, 1967, p. 270.
[22] E.A. Jenne, Geochemical Modeling: A Review, Battelle Pacific Northwest Laboratory, 1981, PNL-3574.
[23] J.D. Hostettler, Am. J. Sci. 284 (1984) 734.
[24] R.D. Lindberg, D.D. Runnells, Science 225 (1984) 925.
[25] A. Stefansson, S. Amorsson, A.E. Sveinbjornsdottir, Chem. Geol. 221 (2005) 289.

[26] ASTM, Standard Specification for Chromium and Chromium–Nickel Stainless Steel Plate, Sheet, and Strip for Pressure Vessels and for General Applications, American Society for Testing and Materials, 2002, A 240/A 240M-02a.
[27] ASTM, Standard Specification for High-Strength, Low-Alloy Structural Steel, up to 50 ksi (345 Mpa) Minimum Yield Point, with Atmospheric Corrosion Resistance, American Society for Testing and Materials, 2005, A 588/A588M-05.
[28] W.J. Weber, J. Nucl. Mater. 98 (1981) 206.
[29] J. Janeczek, R.C. Ewing, V.M. Oversby, L.O. Werme, J. Nucl. Mater. 238 (1996) 121.
[30] D.L. Langmuir, Aqueous Environmental Geochemistry, Prentice-Hall, Upper Saddle River, NJ, 1996.
[31] J.E. Harrar, J.F. Carley, W.F. Isherwood, E. Raber, Report of the Committee to Review the Use of J-13 Well Water in Nevada Nuclear Waste Storage Investigations., Lawrence Livermore National Laboratory, 1990, UCID-21867.
[32] SNL, In-package Chemistry Abstraction, Sandia National Laboratories, 2007, ANL-EBS-MD-000037, Rev 04, Add 01.
[33] L.L. Stookey, Anal. Chem. 42 (1970) 779.
[34] J.H. Pratt, Am. J. Sci. 48 (1984) 149.
[35] A.S. Anastácio, B. Harris, H.-I. Yoo, J.D. Fabris, J.W. Stucki, Geochim. Cosmochim. Acta 72 (2008) 5001.
[36] T.W. Wolery, R.L. Jarek, EQ3NR Speciation-Solubility Code (EQ3/6-V8-EQ3NR-EXE-R43-PC), 2002.
[37] SNL, Qualification of Thermodynamic Data for Geochemical Modeling of Mineral-Water Interations in Dilute Systems, Sandia National Laboratories, 2007, ANL-WIS-GS-0000003, Rev 01.
[38] D.L. Jensen, J.K. Boddum, J.C. Tjell, T.H. Christensen, Appl. Geochem. 17 (2002) 503.
[39] C. Remazeilles, P. Refait, Corros. Sci. 50 (2008) 856.
[40] K. Stahl, K. Nielsen, J.Z. Jiang, B. Lebech, J.C. Hanson, P. Norby, J. van Lanschot, Corros. Sci. 45 (2003) 2563.
[41] U. Schwertmann, H. Fechter, Clay Miner. 29 (1994) 87.
[42] Y. Roh, S.Y. Lee, M.P. Elless, Environ. Geol. 40 (2000) 184.
[43] R. Janot, D. Guerard, J. Alloys Compd. 333 (2002) 302.
[44] T. Ohtsuka, K. Kubo, N. Sato, Corrosion 42 (1986) 476.
[45] J.E. Maslar, W.S. Hurst, W.J. Bowers, J.H. Hendricks, M.I. Aquino, J. Electrochem. Soc. 147 (2000) 2532.
[46] S. Ben Lagha, D. Crusset, I. Mabille, M. Tran, M.C. Bernard, E. Sutter, J. Nucl. Mater. 362 (2007) 485.
[47] S. Music, I. Nowik, M. Ristic, Z. Orehovec, S. Popovic, Croat. Chem. Acta 77 (2004) 141.
[48] J. Kassim, T. Baird, J.R. Fryer, Corros. Sci. 22 (1982) 147.
[49] L. Legrand, S. Savoye, A. Chausse, R. Messina, Electrochim. Acta 46 (2000) 111.
[50] H. Leidheiser, S. Music, Corros. Sci. 22 (1982) 1089.
[51] Y.F. Cheng, F.R. Steward, Corros. Sci. 46 (2004) 2405.
[52] K.E. Garcia, A.L. Morales, C.E. Arroyave, C.A. Barrero, D.C. Cook, Hyperfine Interact. 148 (2003) 177.
[53] S. Savoye, L. Legrand, G. Sagon, S. Lecomte, A. Chausse, R. Messina, P. Toulhoat, Corros. Sci. 43 (2001) 2049.
[54] Y.J. Kim, Corrosion 55 (1999) 81.
[55] S.J. Oh, D.C. Cook, H.E. Townsend, Hyperfine Interact. 112 (1998) 59.
[56] S. McMillian, S. Elkonz, K. Zarrabi, J. Cizdziei, H. Stockman, Abstr. Pap. Am. Chem. Soc. 223 (2002) U614.
[57] D. Neff, P. Dillmann, L. Bellot-Gurlet, G. Beranger, Corros. Sci. 47 (2005) 515.
[58] W.M. Murphy, E.C. Pearcy, R.T. Green, J.D. Prikryl, S. Mohanty, B.W. Leslie, A. Nedungadi, J. Contam. Hydrol. 29 (1998) 245.
[59] W.D. Callister, Material Science and Engineering: An Introduction, John Wiley, New York, 2003.
[60] G. Schikorr, Z. Anorg. Allg. Chem. 212 (1933) 33.
[61] O. Riba, T.B. Scott, K.V. Ragnarsdottir, G.C. Allen, Geochim. Cosmochim. Acta 72 (2008) 4047.
[62] E.C. Pearcy, J.D. Prikryl, W.M. Murphy, B.W. Leslie, Appl. Geochem. 9 (1994) 713.
[63] D.J. Wronkiewicz, J.K. Bates, S.F. Wolf, E.C. Buck, J. Nucl. Mater. 238 (1996) 78.
[64] R.C. Ewing, M.S. Tierney, L.F. Konikow, R.P. Rechard, Risk Anal. 19 (1999) 933.
[65] J. Janeczek, R.C. Ewing, J. Nucl. Mater. 190 (1992) 157.
[66] H.R. Hoekstra, L.H. Fuchs, Science 123 (1956) 105.
[67] L.H. Fuchs, E. Gebert, Am. Mineral. 43 (1958) 243.
[68] L.H. Fuchs, H.R. Hoekstra, Am. Mineral. 44 (1959) 1057.
[69] V. Robit-Pointeau, C. Poinssot, P. Vitorge, B. Grambow, D. Cui, K. Spahiu, H. Catalette, Mat. Res. Soc. Symp. Proc. 932 (2006).
[70] D. Arcos, L.P. del Villar, J. Bruno, C. Domenech, Appl. Geochem. 23 (2008) 807.
[71] K.A. Kubatko, K. Helean, A. Navrotsky, P.C. Burns, Am. Mineral. 91 (2006) 658.
[72] SNL, EBS Radionuclide Transport Abstraction, Sandia National Laboratories, 2007, ANL-WIS-PA_000001, Rev 03.
[73] I. Grenthe, J. Fuger, R. Konings, R.J. Lemire, A.B. Muller, C. Nguyen-Trung, J. Wanner, The Chemical Thermodynamics of Uranium, Elsevier, 1992.
[74] B. Venkataramani, A.R. Gupta, Colloids Surf. 53 (1991) 1.
[75] M.C. Duff, C. Amrhein, Soil Sci. Soc. Am. J. 60 (1996) 1393.
[76] C.K.D. Hsi, D. Langmuir, Geochim. Cosmochim. Acta 49 (1985) 1931.
[77] N. Jaffrezicrenault, H. Poirierandrade, D.H. Trang, J. Chromatogr. 201 (1980) 187.
[78] L. Maya, Radiochim. Acta 31 (1982) 147.
[79] M. Kohler, B.D. Honeyman, J.O. Leckie, Radiochim. Acta 85 (1999) 33.